J. Phys. D: Appl. Phys. 28 (1995) 1856–1868. Printed in the UK

Sadeghi [spec1]

On the use of actinometry to measure the dissociation in O_2 DC glow discharges: determination of the wall recombination probability

D Pagnon, J Amorim, J Nahorny, M Touzeau and M Vialle

Laboratoire de Physique des Gaz et des Plasmas, CNRS, Université Paris XI, 91405 Orsay Cedex, France

Received 20 April 1995

Abstract. A study has been performed to re-investigate the actinometric technique used to determine the absolute concentration of O atoms in DC O_2 flowing glow discharges for pressures ranging from 0.36 to 2 Torr and discharge currents ranging from 5 to 80 mA in Pyrex tubes of three different diameters (16, 7 and 4 mm). Actinometric measurements using $O(^3P - {}^3S)$ 844 nm, $O(^5P - {}^5S)$ 777 nm and $Ar(2p_1 - 1s_2)$ 750 nm transitions are compared to VUV absorption spectrometry. The choice of the excitation cross sections for the calculations of atomic excitation rates as a function of the reduced electric field using a Boltzmann code and the contribution of the quenching processes of the excited states are discussed. The dissociation ratio $[O]/[O_2]$ can be determined from the ratio of intensities I_{844}/I_{750} by the relation $[O]/[O_2] = C_{3P}^{2p1} I_{844}/I_{750}$. We have found that C_{3P}^{2p1} remains constant ($C_{3P}^{2p1} = 2.6 \times 10^{-3}$) throughout the range of experimental conditions investigated. The recombination probability γ of the O atoms at the wall is calculated and correlated to the wall temperature of the Pyrex tubes. The variation of the recombination probability as a function of the wall temperature is fitted by the relation $\gamma = 0.94 \exp(-1780/T_{wall})$ for $300 < T_{wall} < 500$ K.

1. Introduction

Oxygen discharges have been extensively used as sources of oxygen atoms for basic studies in atomic and molecular physics [1, 2], etching and surface treatment [3, 4]. More recently oxygen atom sources have been used in oxidation of high-temperature superconductor thin films in molecular beam epitaxy devices [5, 6] and in the oxidation of YSZ thin films obtained by pulverization [7]. The aim of this work is to investigate the validity of actinometry in the positive column of small diameter O_2 DC glow discharges in order to monitor the flux of atoms in oxygen atom plasma sources of this kind [8–10].

Optical emission actinometry is a widely utilized diagnostic for *in situ* monitoring of spatial and temporal variations of atomic and molecular concentrations [11, 12]. It is easier to handle than optical absorption spectroscopy or laser-induced fluorescence. On the other hand, the validity of actinometry is somewhat controversial and the criteria for the utilization of the technique and its limits of validity must be verified in each case. The validity of actinometry using $O^*(3s\,^3S–3p\,^3P)$ 844 nm and $Ar^*(4s–4p)$ 750 nm transitions was investigated by Walkup *et al* [13]. They found that the actinometric determination was well correlated with the variation of atom concentration in 0.4 Torr RF O_2–CF_4 plasmas, but discrepancies occurred in pure O_2 plasmas. Booth *et al* [14] have shown that the ratio of the intensities of the oxygen line to the argon line, I_{O*} (844 nm)/I_{Ar*} (750 nm), was poorly correlated to the oxygen atom concentration in ECR low-pressure (1–6 mTorr) plasmas containing O_2. The fact that the ratio of intensities was well correlated with $[O_2]$ was interpreted by considering that the most important mechanism of production of the 844 nm line is dissociative excitation when dissociation rates are lower than 0.1. Breithbarth *et al* [15] proved the validity of actinometry in RF O_2–CF_4 plasmas with an applied electric field. Granier *et al* [16] have shown that actinometry can be used to monitor the atom concentration in O_2 and O_2–N_2 low-pressure (0.5–2 Torr) microwave plasmas. A new method, time-resolved actinometry has recently been developed in modulated plasmas to study the kinetics of hydrogen–argon plasmas [17] or fluorinated plasmas [18]. This technique has been applied to O_2 and O_2–SF_6 or F_2 ECR plasmas by Booth and Sadeghi [19], who concluded that the determination of oxygen atom concentrations was impossible from observation of the 844 nm line because the production of emitting atoms $O(3p\,^3P)$ (844 nm) is principally due to dissociative excitation of O_2. The same

0022-3727/95/091856+13$19.50

conclusion was obtained in pulsed RF low-pressure O_2 plasmas by Collart *et al* [4], who suggested that highly energetic electrons are responsible for the dissociative excitation of O_2. It appears then that the validity of actinometry technique strongly depends on the experimental conditions.

In the present work, we have determined the concentration of oxygen atoms in the positive column of a glow discharge created in Pyrex tubes of three different diameters (16, 7 and 4 mm). The actinometric technique using the classical $O(^3P–^3S)$ 844 nm, $O(^5P–^5S)$ 777 nm and $Ar(2p_1–1s_2)$ 750 nm transitions is discussed in detail for these experimental conditions in section 2. The values of the excitation rate of the $O(^5P)$, $O(^3P)$ and $Ar(2p_1)$ states are calculated as a function of the reduced electric field E/N using a Boltzmann code which had been developed previously [20]. The contribution of the dissociative excitation of the O_2 molecules which can contribute to an inaccuracy in the determination of the oxygen atom concentration is evaluated. The importance of the quenching processes of the excited states is also discussed. In section 3, we present a comparison of the dissociation ratio determined by actinometry and by VUV absorption and we show that we obtain a good agreement between these two techniques. The actinometry technique was used to determine the dissociation ratio in small-diameter tubes for which the VUV technique is difficult to utilize. The results of the dissociation ratios obtained in the tubes of three different diameters are compared in section 4. These measurements show that a saturation of the dissociation ratio is obtain in small-diameter tubes when the discharge current increases. This behaviour is interpreted in section 5 as the result of the balance between the production of atoms by dissociative electronic impact and their loss by recombination at the wall.

2. Determination of the concentration of ground state oxygen atoms by actinometry

2.1. Principles

In order to determine the concentration of ground state oxygen atoms, we have used the classical technique which consists of comparing the emission of the $O(^3P–^3S)$ 844 nm and $O(^5P–^5S)$ 777 nm transitions to the emission of the $Ar(2p_1–1s_2)$ 750 nm transition (figure 1).

We suppose that these X_i^* states are mainly populated by electron impact from the ground state X:

$$e + X \xrightarrow{k_e^{X_i}} X_i^* + e. \tag{1}$$

The de-excitation of excited states X_i^* is either radiative:

$$X_i^* \xrightarrow{A_{ij}} X_j^* + h\nu_{ij} \tag{2}$$

or non-radiative by quenching with species Q (Q = O_2, O or Ar):

$$X_i^* + Q \xrightarrow{k_Q} X + Q. \tag{3}$$

$$X_i^* + O_2 \xrightarrow{k_3} X + O_2$$

$$X_i^* + Ar \xrightarrow{k_3} X + Ar$$

The emission intensity I_{X^*} of a transition $X_i^* \rightarrow X_j^*$ is then written as the ratio between production and loss processes:

$$I_{X^*} = C\frac{h\nu_{ij}A_{ij}k_e^{X_i}n_e}{(\Sigma A_{ij} + k_Q[Q])}[X] \tag{4}$$

where n_e is the electronic density, $h\nu_{ij}$ is the energy of the emited photon (relation (2)), A_{ij} is the Einstein coefficient for the observed transition ($i \rightarrow j$), ΣA_{ij} is the sum of all radiative de-excitation processes of the ith level, and C represents a constant dependent on the detection system (in the following, we take the same C value for all emission lines because the volume observed by the optical system is the same). The coefficient $k_e^{X_i}$ can be expressed by the following relation:

$$k_e^{X_i} = \left(\frac{2e}{m}\right)^{1/2}\int_{\epsilon_{th}}^{\infty} v(\epsilon)\sigma_i(\epsilon)f(\epsilon)\,d\epsilon \tag{5}$$

where $v(\epsilon)$ is the electron velocity, $\sigma_i(\epsilon)$ is the collision cross section with threshold energy ϵ_{th} for excitation of level i (relation (1)) and $f(\epsilon)$ is the electron energy distribution function (EEDF) normalized by

$$\int_0^{\infty} f(\epsilon)\epsilon^{1/2}\,d\epsilon = 1. \tag{6}$$

With the relation (5), relation (4) becomes

$$I_{X^*} = Ch\nu_{ij}A_{ij}\int_{\epsilon_{th}}^{\infty} v(\epsilon)\sigma_i(\epsilon)f(\epsilon)\,d\epsilon\frac{n_e[X]}{\Sigma A_{ij} + k_Q[Q]}. \tag{7}$$

As we can see, the intensity relies on the electron density and the electron distribution function. It is possible to compensate the variations in n_e by dividing the emission intensity of an oxygen line by the intensity of the actinometer line (in our case the 750.4 nm line of argon), thus

$$\frac{I_{O^*}}{I_{Ar^*}} = \frac{h\nu_{ij}^O A_{ij}^O}{h\nu_{ij}^{Ar}A_{ij}^{Ar}}\frac{k_e^O}{k_e^{Ar}}\frac{(\Sigma A_{ij}^{Ar} + k_Q^{Ar}[Q])}{(\Sigma A_{ij}^O + k_Q^O[Q])}\frac{[O_2]}{[Ar]}\frac{[O]}{[O_2]}$$

$$= \frac{1}{C_O^{Ar}}\frac{[O]}{[O_2]} \tag{8}$$

where

$$C_O^{Ar} = \frac{h\nu_{ij}^{Ar}A_{ij}^{Ar}}{h\nu_{ij}^O A_{ij}^O}\frac{k_e^{Ar}}{k_e^O}\frac{\Sigma A_{ij}^O + k_Q^O[Q]}{\Sigma A_{ij}^{Ar} + k_Q^{Ar}[Q]}\frac{[Ar]}{[O_2]}.$$

Hence the ratio of the intensities I_O/I_{Ar} is proportional to the $[O]/[O_2]$ concentration ratio if the coefficient C_O^{Ar} remains constant throughout the experimental range.

2.2. The influence of the dissociative electronic excitation of $O(3p\,^3P)$ and $O(3p\,^5P)$

Under our experimental conditions the $Ar(2p_1)$ excited state of argon is populated by direct electronic impact from ground state:

$$e + Ar(1p_0) \xrightarrow{k_e^{2p_1}} Ar(2p_1) + e. \tag{9}$$

The stepwise excitation by metastable Ar states can be neglected because the metastable states are destroyed by collision with the oxygen molecules [21].

To yield oxygen excited states $O(3p\,^3P)$ and $O(3p\,^5P)$, two channels have to be taken into account:

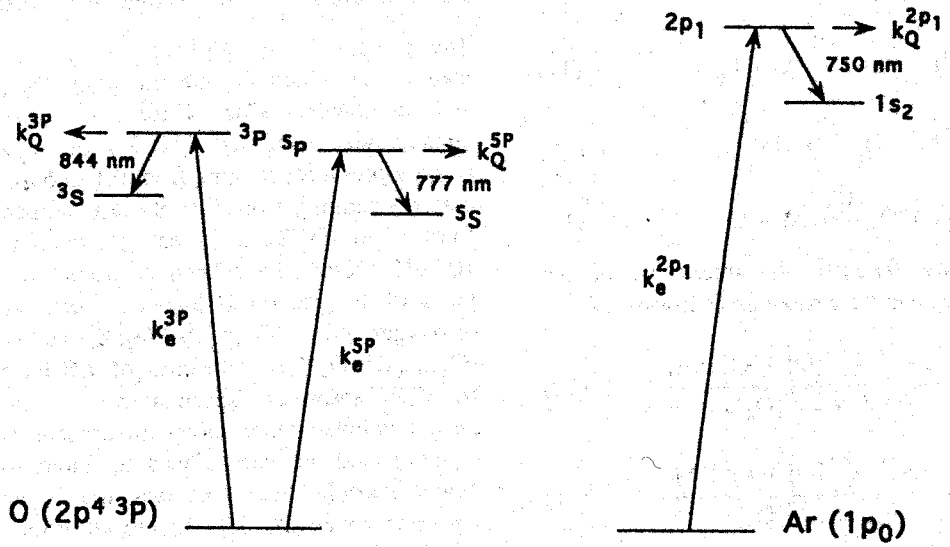

Figure 1. A schematic diagram of the excited levels involved in the determination of the concentration of ground state atoms by actinometry.

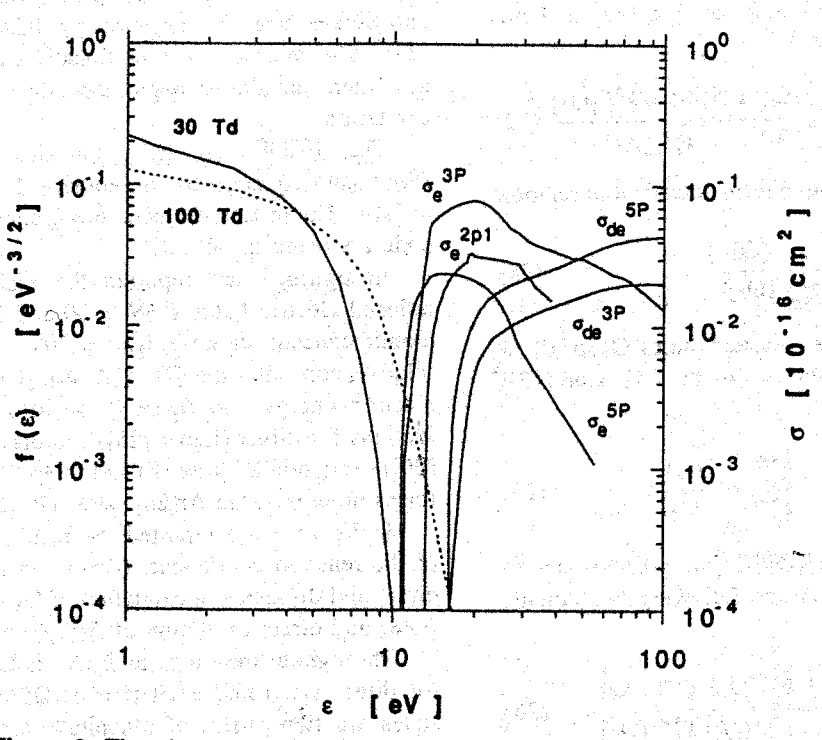

Figure 2. The electron energy distribution function calculated for $E/N = 30$ (full line) and 100 Td (broken line) versus the electron energy. The cross sections for direct excitation of Ar($2p_1$), σ_e^{2p1}; O(^{3}P), σ_e^{3P}; and O(^{5}P), σ_e^{5P} and for dissociative excitation of O(^{3}P), σ_{de}^{3P}; and O(^{5}P), σ_{de}^{5P} are also reported.

(i) direct electronic impact with ground state atoms:

$$e + O(2p^4\,{}^3P) \xrightarrow{k_e^{3P}} O(3p\,{}^3P) + e \qquad (10)$$

$$e + O(2p^4\,{}^3P) \xrightarrow{k_e^{5P}} O(3p\,{}^5P) + e \qquad (11)$$

(ii) dissociative excitation by electronic collisions from the ground state molecules:

$$e + O_2 \xrightarrow{k_{de}^{3P}} O + O(3p\,{}^3P) + e \qquad (12)$$

$$e + O_2 \xrightarrow{k_{de}^{5P}} O + O(3p\,{}^5P) + e. \qquad (13)$$

The excited states are depopulated by radiative de-excitation:

$$O(3p\,{}^3P) \xrightarrow{A_{ij}^{3P}} O(3s\,{}^3S) + h\nu(844.6\text{ nm}) \qquad (14)$$

$$O(3p\,{}^5P) \xrightarrow{A_{ij}^{5P}} O(3s\,{}^5S) + h\nu(777.4\text{ nm}) \qquad (15)$$

$$Ar(2p_1) \xrightarrow{A_{ij}^{2p_1}} Ar(1p_0) + h\nu(750.4\text{ nm}) \qquad (16)$$

and by quenching with oxygen molecules:

$$O(3p\,^3P) + O_2 \xrightarrow{k_Q^{3P}} O + O_2 \quad (17)$$

$$O(3p\,^5P) + O_2 \xrightarrow{k_Q^{5P}} O + O_2 \quad (18)$$

$$Ar(2p_1) + O_2 \xrightarrow{k_Q^{2p_1}} Ar + O_2. \quad (19)$$

From the relations (9)–(19), the intensities of the oxygen and argon lines can be written as follows:

$$I_{844} = \frac{n_e h\nu_{844} A_{ij}^{3P}(k_e^{3P}[O] + k_{de}^{3P}[O_2])}{\Sigma A_{ij}^{3P} + k_Q^{3P}[O_2]} \quad (20)$$

$$I_{777} = \frac{n_e h\nu_{777} A_{ij}^{5P}(k_e^{5P}[O] + k_{de}^{5P}[O_2])}{\Sigma A_{ij}^{5P} + k_Q^{5P}[O_2]} \quad (21)$$

$$I_{750} = \frac{n_e h\nu_{750} A_{ij}^{2p_1} k_e^{2p_1}[Ar]}{\Sigma A_{ij}^{2p_1} + k_Q^{2p_1}[O_2]}. \quad (22)$$

The ratio of the intensity of one oxygen line, 844 nm for example, to the argon line is

$$\frac{I_{844}}{I_{750}} = \frac{h\nu_{844} A_{ij}^{3P}}{h\nu_{750} A_{ij}^{2p_1}} \frac{\Sigma A_{ij}^{2p_1} + k_Q^{2p_1}[O_2]}{\Sigma A_{ij}^{3P} + k_Q^{3P}[O_2]} \frac{k_e^{3P}[O] + k_{de}^{3P}[O_2]}{k_e^{2p_1}[Ar]} \quad (23)$$

and it can be written in the simple form described in relation (8):

$$\frac{I_{844}}{I_{750}} = \frac{1}{C_{3P}^{2p_1}} \frac{[O]}{[O_2]} \quad (24)$$

only when the yield of oxygen excited states $O(3p\,^3P)$ or $O(3p\,^5P)$ by dissociative excitation (relation (12) or (13)) is negligible:

$$\frac{k_{de}^{3P}}{k_e^{3P}} \quad \text{or} \quad \frac{k_{de}^{5P}}{k_e^{5P}} \ll \frac{[O]}{[O_2]}. \quad (25)$$

Then, the concentration ratio $[O]/[O_2]$ is proportional to the ratio of the intensities when the following coefficients remain constant:

$$C_{3P}^{2p_1} = \frac{h\nu_{750} A_{ij}^{2p_1}}{h\nu_{844} A_{ij}^{3P}} \frac{\Sigma A_{ij}^{3P} + k_Q^{3P}[O_2]}{\Sigma A_{ij}^{2p_1} + k_Q^{2p_1}[O_2]} \frac{k_e^{2p_1}}{k_e^{3P}} \frac{[Ar]}{[O_2]} \quad (26)$$

$$C_{5P}^{2p_1} = \frac{h\nu_{750} A_{ij}^{2p_1}}{h\nu_{777} A_{ij}^{5P}} \frac{\Sigma A_{ij}^{5P} + k_Q^{5P}[O_2]}{\Sigma A_{ij}^{2p_1} + k_Q^{2p_1}[O_2]} \frac{k_e^{2p_1}}{k_e^{5P}} \frac{[Ar]}{[O_2]}. \quad (27)$$

So, in order to discuss the validity of the actinometric method, we have calculated the coefficients $C_{3P}^{2p_1}$ and $C_{5P}^{2p_1}$ and the ratios k_{de}^{3P}/k_e^{3P} and k_{de}^{5P}/k_e^{5P}. We have then calculated the electron energy distribution function under our experimental conditions. With this EEDF, we have determined the different rate coefficients (k_e^{3P}, k_e^{5P}, k_{de}^{3P}, k_{de}^{5P} and $k_e^{2p_1}$), using relation (5) and different sets of collisional cross sections for each excited state in order to evaluate the importance of the choice of a cross section. The influence of the quenching processes (relations (17)–(19)) is also discussed in the following.

2.3. Calculation of the excited states rate coefficients

The plasma of the positive column is a homogeneous medium in which the electric field, the gas temperature and the concentration of the main active species have already been measured with a good accuracy [22]. For oxygen pressures ranging from 0.1 to 5 Torr and discharge currents ranging from 5 to 80 mA, reduced electric fields from 30 to 100 Td and electronic density of the order of 10^{10}–10^{11} cm^{-3} have been measured in Pyrex discharge tubes of 16 mm inner diameter. Relative concentrations of oxygen atoms $[O(3p\,^3P)]/[O_2(X)]$ and singlet molecules $[O_2(a^1\Delta)]/[O_2(X)]$ of the order of 10% have been measured by VUV absorption spectroscopy. A kinetic model has been developed which solves simultaneously the Boltzmann equation and the rate balance equations for the dominant heavy particles and describes the experimental results reasonably well [20, 23]. As a result of the large quenching of vibrationally excited O_2 molecules by oxygen atoms, we have assumed in this model that the vibrational temperature is equal to the gas temperature. This assumption has been verified under our experimental conditions by coherent anti-Stokes Raman spectroscopy (CARS) measurements [24]. The presence of vibrationally excited O_2 molecules has, then, an almost negligible effect on the dissociative excitation.

The EEDF has been calculated by solving the Boltzmann equation by the numerical approach developed in [20]. The processes taken into account in the Boltzmann code are listed in table 1.

In figure 2 are reported the EEDFs calculated for reduced electric fields $E/N = 30$ and 100 Td, for relative atomic concentration $[O]/[O_2] = 10\%$ and singlet molecule relative concentration $[O_2(a^1\Delta)]/[O_2] = 10\%$, versus the electron energy. In figure 2 are also reported the cross sections for direct (Laher [25]) and dissociative (Schulman [26]) excitation of $O(3p\,^3P)$ and $O(3p\,^5P)$ oxygen states and for excitation of the $Ar(2p_1)$ state (Puech [27]).

In figure 3 are reported the results of the calculation of the reaction coefficients (according to relation (5)), for direct and dissociative excitation of $O(3p\,^3P)$ and $O(3p\,^5P)$ states and direct excitation of $Ar(2p_1)$ state.

Throughout the range of E/N studied, the coefficients for direct electronic excitation of $O(3p\,^3P)$ and $O(3p\,^5P)$ states are two orders of magnitude larger than those for dissociative excitation. It can be observed in figure 3 that the values of the excitation rate are very sensitive to the shape of the cross sections near the threshold energy.

In order to estimate the uncertainties due to our choice of cross section, we have calculated each rate coefficient with two different cross sections from the literature. The comparisons between the cross sections from Laher *et al* [25] and Julienne *et al* [34] for excitation of $O(3p\,^3P)$ or $O(3p\,^5P)$ and of the cross sections from Puech *et al* [27] and Ballou *et al* [35] for excitation of $Ar(2p_1)$ are reported in figure 4.

Calculations of the argon to oxygen excitation rate coefficients ratios k_e^{2p1}/k_e^{5P} and k_e^{2p1}/k_e^{3P} lead to results presented in figure 5 for reduced electric field E/N ranging from 30 to 100 Td. In figures 4 and 5, the following two facts are evident.

Table 1. Inelastic and superelastic collision processes considered in the Boltzmann equation, and corresponding references to the cross section data.

Electron processes		Reference
Molecular oxygen		
(R1)	$e + O_2(X, v) \rightleftharpoons e + O_2(X, w)$	[28]
(R2)	$e + O_2(X, v = 0) \rightleftharpoons e + O_2(a^1\Delta)$	[28]
(R3)	$e + O_2(X, v = 0) \rightleftharpoons e + O_2(b^1\Sigma)$	[28]
(R4)	$e + O_2(X, v = 0) \rightarrow e + O_2(4.5\ eV)$	[28]
(R5)	$e + O_2(X, v = 0) \rightarrow e + O_2(6.0\ eV)$	[28]
(R6)	$e + O_2(X, v = 0) \rightarrow e + O_2(8.4\ eV)$	[28]
(R7)	$e + O_2(X, v = 0) \rightarrow e + O_2(9.97\ eV)$	[28]
(R8)	$e + O_2(X, v = 0) \rightarrow e + e + O_2^+$	[28]
(R9)	$e + O_2(X, v = 0) \rightarrow e + O_2(14.7\ eV)$	[28]
(R10)	$e + O_2(a^1\Delta) \rightleftharpoons e + O_2(b^1\Sigma)$	[29]
(R11)	$e + O_2(a^1\Delta) \rightarrow e + e + O_2^+$	
(R12)	$e + O_2(b^1\Sigma) \rightarrow e + e + O_2^+$	
(R13)	$e + O_2(X, v = 0) \rightarrow O(3p\,^3P) + O(^3P) + e$	
(R14)	$e + O_2(X, v = 0) \rightarrow O(3p\,^5P) + O(^3P) + e$	
Atomic oxygen		
(R15)	$e + O(^3P) \rightleftharpoons e + O(^1D)$	[30]
(R16)	$e + O(^3P) \rightleftharpoons e + O(^1S)$	[30]
(R17)	$e + O(^3P) \rightarrow e + O(^3S)$	[31]
(R18)	$e + O(^1D) \rightleftharpoons e + e + O(^1S)$	[30]
(R19)	$e + O(^3P) \rightarrow e + e + O^+$	[32]
(R20)	$e + O(^1D) \rightarrow e + e + O^+$	[33]
(R21)	$e + O(^1S) \rightarrow e + e + O^+$	[33]
(R22)	$e + O(^3P) \rightarrow O(3p\,^3P) + e$	Text
(R23)	$e + O(^3P) \rightarrow O(3p\,^5P) + e$	Text
Argon		
(R24)	$e + Ar(1p_0) \rightarrow e + Ar(2p_1)$	Text

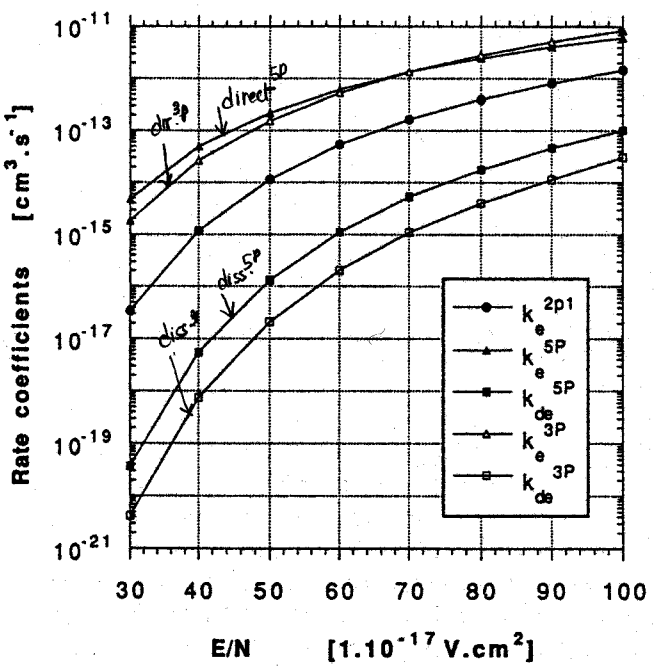

Figure 3. Reaction rates for direct and dissociative electronic excitation of $O(3p\,^3P)$ and $O(3p\,^5P)$ and direct electronic excitation of $Ar(2p_1)$ states.

(i) At low E/N (30–40 Td), the large difference between calculated ratios k_e^{2p1}/k_e^{5P} or k_e^{2p1}/k_e^{3P} can be explained in terms of different rising fronts in the cross sections near threshold energies. At high E/N (90–100 Td) we also obtain a large difference due to different shapes of the various cross sections. At medium E/N (50–80 Td), the two causes of difference compensate each other and the resulting difference is minimized. We will see in the following that the best fit between VUV and actinometric $[O]/[O_2]$ concentration ratio measurements is obtained with the $Ar(2p_1)$ Puech cross section and $O(3p\,^3P)$ and $O(3p\,^5P)$ Laher cross sections.

(ii) An uncertainty in the determination of reduced electric field E/N, which is principally due to the determination of gas temperature, introduces an error into the determination of ratios $k_e^{2p_1}/k_e^{5P}$ or k_e^{2p1}/k_e^{3P}. An error of $\pm 10\%$ in the reduced electric field E/N leads to an error of $\pm 20\%$ in the ratios for $E/N \geq 70$ Td and of $\pm 35\%$ for $E/N < 60$ Td. For values of $E/N < 40$ Td the calculation is imprecise because it only uses the rising front of the cross section near the threshold.

2.4. Quenching of the excited states

In order to express the ratios I_{844}/I_{750} and I_{777}/I_{750} versus $[O]/[O_2]$ (according to relations (23) and (24)) with coefficients C_{2p}^{3P} and C_{2p}^{5P} expressed in relations (26) and (27), we have also evaluated the quenching of excited atomic states by oxygen molecules (relations (17)–(19)). For the $O(3p\,^3P)$ excited state, Dagdigian *et al* [36] obtained by laser-induced fluorescence emission of the 3P state upon two-photon excitation a radiative decay rate $\Sigma A_{ij}^{3P} = 2.98 \times 10^7\ s^{-1}$ which agrees well with other determinations (for example by Bamford [37] and Bittner

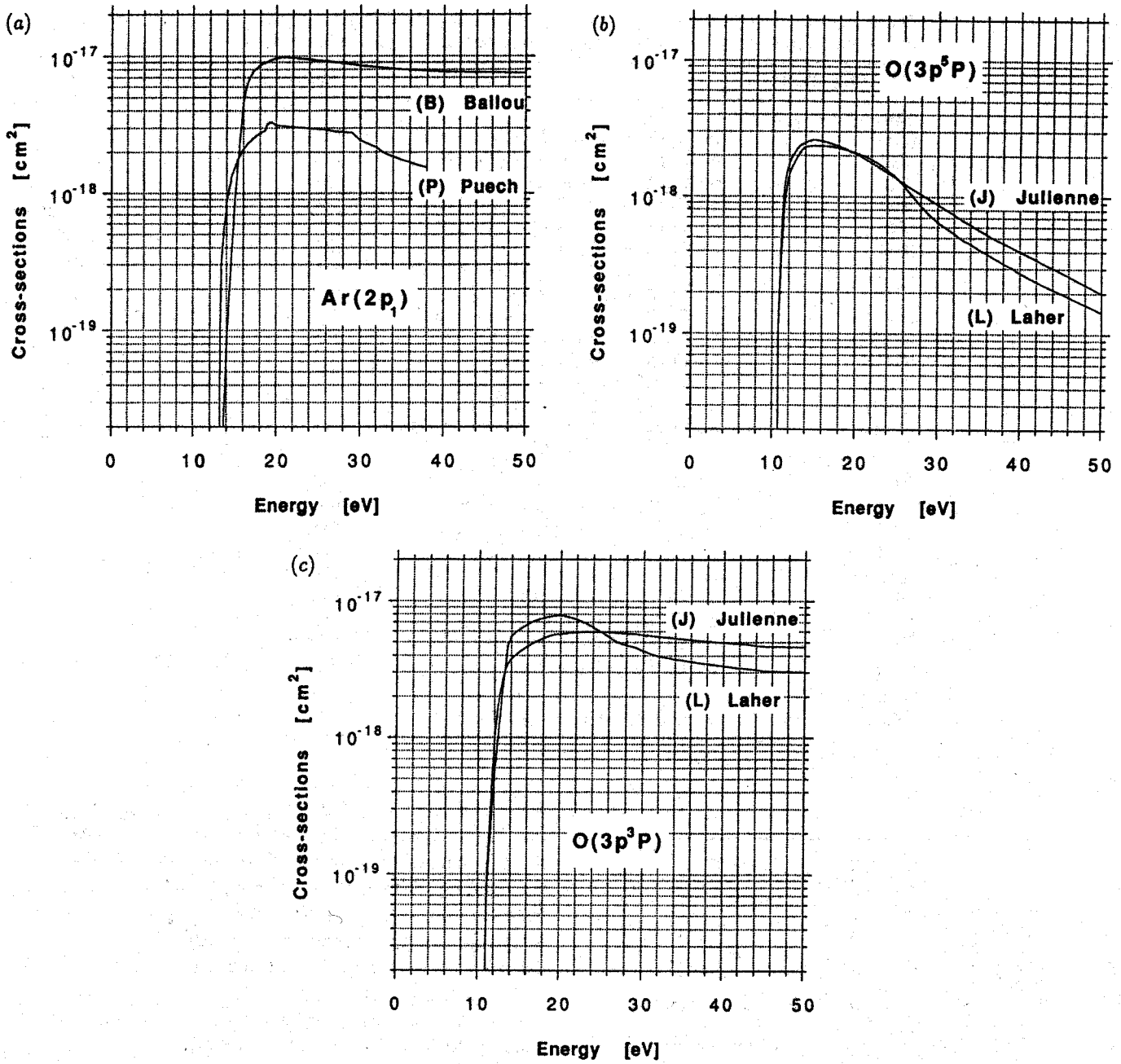

Figure 4. A comparison of the cross sections for direct electronic excitation of $Ar(2p_1)$ (*a*), $O(3p\,^5P)$ (*b*) and $O(3p\,^3P)$ (*c*) versus energy given by Ballou [34], Puech [26], Julienne [33] and Laher [24].

[38]). This is also the value of the transition probability at 844 nm since the $O(3p\,^3P)$ state has only one electric-dipole-allowed decay pathway. These authors deduced a quenching rate of the $O(3p\,^3P)$ state by O_2 molecules, $k_Q^{3P} = 7.8 \times 10^{-10}$ mol^{-1} cm^3 s^{-1}, and surmise that the bulk of ^3P quenching collisions occur by excitation transfer to the O_2 molecule partner rather than collision-induced transitions to lower lying oxygen atom states.

By taking the quenching rates k_Q^{3P} and k_Q^{5P} of Dagdigian, and comparing the actinometric and the VUV measurements (section 3), we have found that the best fit is obtained throughout the range of pressure and current when

$$k_Q^{3P}[O_2] = 2.6 \times 10^7 p \text{ (Torr s}^{-1}\text{)}$$
$$k_Q^{5P}[O_2] = 3.5 \times 10^7 p \text{ (Torr s}^{-1}\text{)} \quad (28)$$

namely with a quenching rate constant that increases linearly with the gas temperature. The quenching rate constant k_Q^{2p1} of the argon excited state $Ar(2p_1)$ by O_2 molecules has been measured by Belikov *et al* [39] for gas temperatures ranging from 95 to 210 K. They obtain a quenching rate constant $k_Q^{2p1} = 0.9T^{-0.63} \times 10^{-10}$ cm^3 s^{-1}. Insofar as we can extrapolate this temperature law under our experimental conditions, we obtain for $300 < T < 600$ K

$$8.1 \times 10^6 p \text{ (Torr s}^{-1}\text{)} \geq k_Q^{2p1}[O_2] \geq 2.6 \times 10^6 p \text{ (Torr s}^{-1}\text{)}. \quad (29)$$

Because these $k_Q^{2p1}[O_2]$ values are lower than the uncertainty in the radiative decay rate $\Sigma A_{ij}^{3P} = 4.4 \times 10^7$ s^{-1}, we have neglected the quenching of the argon excited state $Ar(2p_1)$ by O_2 molecules in our calculations.

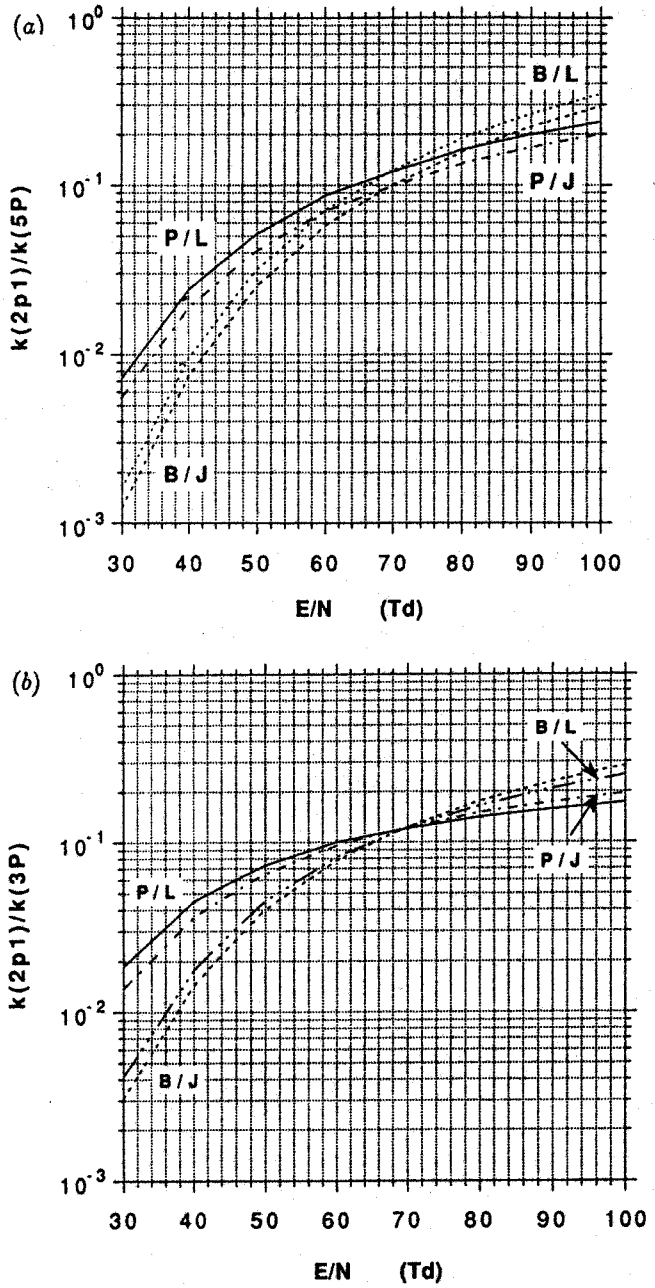

Figure 5. Values of $k_e^{2p_1}/k_e^{5P}$ (*a*) and $k_e^{2p_1}/k_e^{3P}$ (*b*) calculated using the cross sections of Puech and Laher (P/L), Ballou and Laher (B/L), Puech and Julienne (P/J) and Ballou and Julienne (B/J).

The values of $C_{3P}^{2p_1}$ and $C_{5P}^{2p_1}$ coefficients calculated (relations (26) and (27)) with these quenching values under our experimental conditions are reported in table 2.

3. Comparison with VUV absorption measurements

The experiments were performed by measuring the emissions of $O(3p^3P)$ and $O(3p^5P)$ excited oxygen atoms and $Ar(2p_1)$ argon lines in the positive column of a DC discharge. The experimental device reported in figure 6 allows simultaneous measurements by VUV absorption spectrometry and by actinometry. The light emitted by the discharge is focused at the entrance slit of an optical multichannel analyser (OMA). The VUV absorption technique has been described in detail elsewhere [22, 23].

The DC discharge is excited in a 16 mm inner diameter Pyrex tube containing an O_2–Ar mixture $([Ar]/[O_2]) = 10^{-2}$. The pressures range from 0.3 to 2 Torr and the discharge currents from 5 to 80 mA. The reduced electric field E/N is determined by measuring the sustained electric field E using two Langmuir probes and the gas temperature is deduced from the rotational emission distribution of the 760 nm atmospheric band $O_2(b^1\Sigma\text{–}X^3\Sigma)$ by the method described in detail in [40].

In figure 7 are reported the values of the dissociation ratio $[O]/[O_2]$ measured by VUV absorption spectroscopy and actinometry versus the discharge current for 0.36 and 0.56 Torr. We obtain a good agreement with VUV measurements for the two sets of determinations using $O(3p^3P)$ (±30%) or $O(3p^5P)$ (±20%) throughout the range of pressure investigated.

As shown in figure 8, the values deduced from actinometric measurements are larger than those obtained from VUV absorption. This discrepancy is important at low current and low pressure because under these conditions the reduced electric field is high, yielding energetic electrons able to induce dissociative excitation and the concentration $[O]/[O_2]$ is below 1%. We have thus to take into account the production of atomic excited states $O(3p^5P)$ by dissociative excitation (relation (13)). For this excited state the intensity ratio is

$$\frac{I_{777}}{I_{750}} = \frac{h\nu_{777}A_{ij}^{5P}}{h\nu_{750}A_{ij}^{2p_1}} \frac{\Sigma A_{ij}^{2p_1}}{\Sigma A_{ij}^{5P} + k_Q^{5P}[O_2]} \frac{k_e^{5P}[O] + k_{de}^{5P}[O_2]}{k_e^{2p_1}[Ar]}. \quad (30)$$

Using this relation, we can express the concentration ratio $[O]/[O_2]$ versus the intensities ratio by

$$\frac{[O]}{[O_2]} = C_{5P}^{2p_1}\left(\frac{I_{777}}{I_{750}}\right) - \frac{k_{de}^{5P}}{k_e^{5P}} \quad (31)$$

where the $C_{5P}^{2p_1}$ coefficient is defined by relation (27). Calculations of the ratio k_{de}^{5P}/k_e^{5P} are performed using the calculated EEDF and the cross sections from Schulman [26] for dissociative excitation and Laher [25] for direct excitation of the $O(3p^5P)$ excited state (figure 9). Taking into account this correction, it can be shown in figure 8 that the discrepancy is then lower than 30%.

We can conclude, from this study of a DC glow discharge in O_2 (1% Ar) in a 16 mm diameter Pyrex tube, that actinometry can lead to absolute $[O]/[O_2]$ concentration ratios with a good accuracy for current ranging from 5 to 80 mA and pressure from 0.36 to 2 Torr. Perturbation due to dissociative excitation can be minimized by choosing the $O(3p^3P)$ state instead of $O(3p^5P)$. In fact, as we can see in figure 9, the ratio k_{de}/k_e for $O(3p^3P)$ is one order of magnitude smaller than that for $O(3p^5P)$. Because the quenching rate is also better determined for $O(3p^3P)$ than for $O(3p^5P)$, and the coefficient $C_{3P}^{2p_1}$ $(2.10 \times 10^{-3} \pm 7\%)$ is constant throughout the range of our experimental conditions, it is preferable to choose the $O(3p^3P) \rightarrow O(3s^3S)$ transition (844 nm) to determine the absolute concentration ratio $[O]/[O_2]$ by actinometry.

Table 2. Variation of C_{3P}^{2p1} and C_{5P}^{2p1} versus the pressure.

	Pressure (Torr)				
Coefficients	0.36	0.56	1	2	Mean value
$C_{3P}^{2p_1}$	2.09×10^{-3}	1.98×10^{-3}	2.09×10^{-3}	2.25×10^{-3}	2.10×10^{-3} (±7%)
$C_{5P}^{2p_1}$	2.24×10^{-3}	1.86×10^{-3}	1.75×10^{-3}	1.63×10^{-3}	1.87×10^{-3} (±20%)

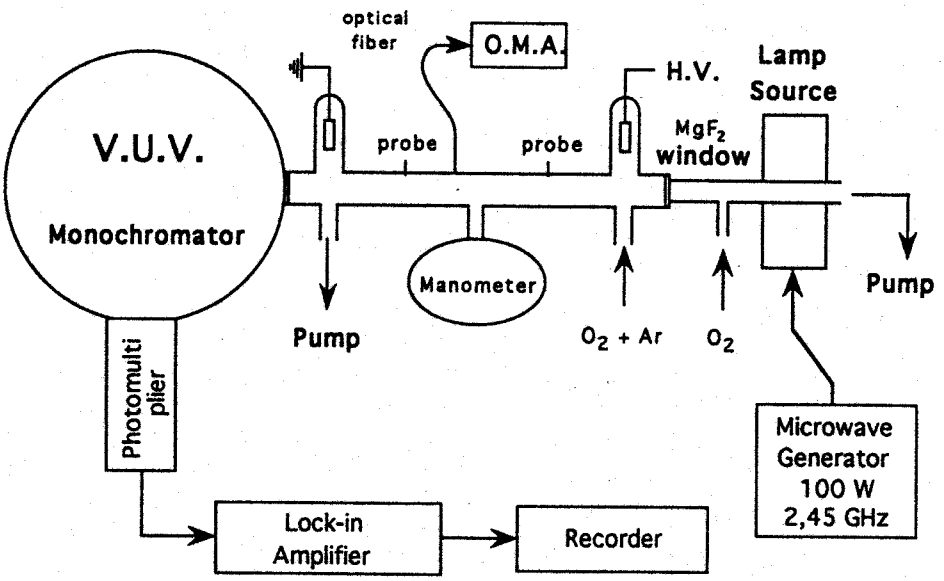

Figure 6. The experimental set-up for actinometry and VUV absorption spectrometry.

Table 3. A comparison between measured and 'calculated' reduced electric field in a 7 mm diameter tube for a pressure of 1 Torr.

I_d (mA)	Calculated E/N (Td)	Measured E/N (Td)
10	95.0	
20	87.0	93.0
30	84.6	87.3
40	88.1	96.8
50	88.3	96.1
60	88.5	102.3
70	84.6	
80	83.2	103.7
100	83.4	

4. Actinometry in 7 and 4 mm diameter tubes

In order to design sources of atomic species (O, H and N), we have used small-diameter tubes. Because we are in this case principally interested in the yield of oxygen atoms, and VUV absorption measurements are difficult to perform in these tubes, we have used the actinometric method to determine $[O]/[O_2]$ concentration ratios in 7 and 4 mm inner diameter discharge tubes, for a pressure of 1 Torr and currents ranging from 10 to 100 mA. For these small-diameter tubes, the reduced electric field E/N has been deduced from the intensities of the 844 and 777 nm lines.

From relations (20) and (21) describing these intensities, we can write the intensities ratio as

$$\frac{I_{844}}{I_{777}} = \frac{h\nu_{844}A_{ij}^{3P}}{h\nu_{777}A_{ij}^{5P}} \frac{\Sigma A_{ij}^{5P} + k_Q^{5P}[O_2]}{\Sigma A_{ij}^{3P} + k_Q^{3P}[O_2]} \frac{k_e^{3P}}{k_e^{5P}}. \quad (32)$$

On taking into account the quenching for 1 Torr of the two excited states as discussed previously, we obtain

$$\frac{I_{844}}{I_{777}} = 1.13 \times \frac{k_e^{3P}}{k_e^{5P}} \quad (33)$$

and so, from the measurement of the intensities of 844 and 777 nm emission lines, we can determine the ratio k_e^{3P}/k_e^{5P} and deduce the reduced electric field E/N leading to this ratio. From the values of E/N obtained, we have calculated the k_e^{2p1}, k_e^{3P} and k_e^{5P} rate coefficients and then the ratios k_e^{2p1}/k_e^{3P} and k_e^{2p1}/k_e^{5P} involved in the C_{3P}^{2p1} and C_{5P}^{2p1} coefficients (relations (26) and (27)). Concentrations $[O]/[O_2]$ are obtained using relation (24) for the $O(3p\,^3P) \rightarrow O(3s\,^3S)$ transition and a similar relation for the $O(3p\,^5P) \rightarrow O(3s\,^5S)$ transition (844 and 777 nm respectively). In order to validate this method, we have tested it on the 7 mm diameter tube in which the reduced electric field E/N has been measured.

In table 3 the values of the reduced electric field measured in the 7 mm tube are compared to that deduced from relation (33) for discharge currents ranging from 10 to 100 mA. The error in the measured E/N values is of the order of 20%.

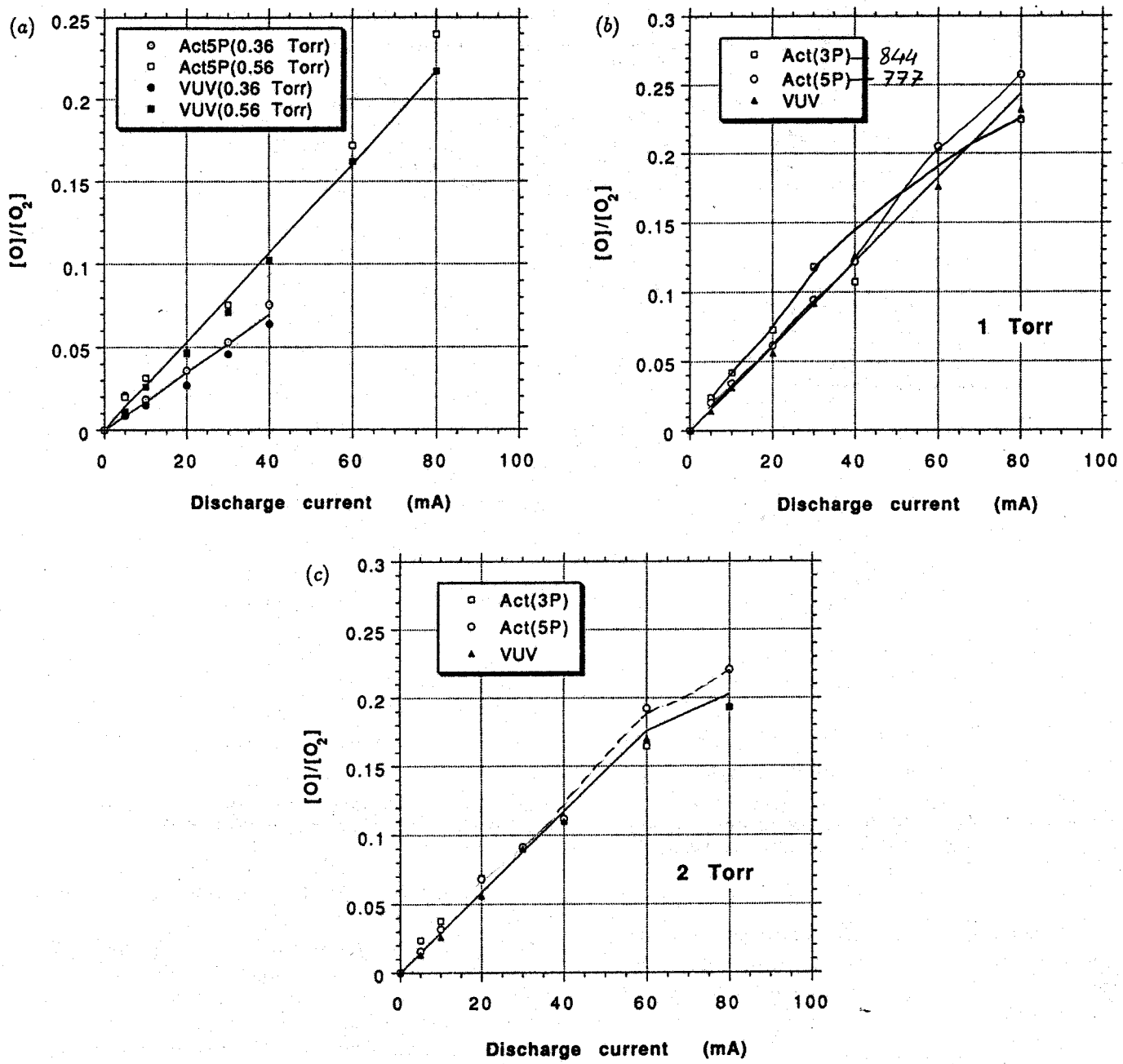

Figure 7. A comparison of the dissociation ratio [O]/[O_2] determined by actinometry (Act3P using the 844 nm line, Act5P using the 777 nm line) and VUV measurements for 0.36 and 0.56 (*a*); 1 (*b*) and 2 Torr (*c*).

The reduced electric fields E/N deduced from relation (33) compare well with the measured values with discrepancies lower than 20%. The ratios k_e^{2p1}/k_e^{3P} and k_e^{2p1}/k_e^{5P} are then deduced from the values of E/N corresponding to each discharge current. The [O]/[O_2] concentration ratios are deduced from relation (24) using the coefficients C_{5P}^{2p1} and C_{3P}^{2p1} calculated from relations (26) and (27) and listed in table 4.

In figure 10(*a*) are represented the [O]/[O_2] concentration ratios resulting from measured E/N and from E/N deduced from relation (33). If we calculate the mean value between the two determinations, we obtain an accuracy of ±20%.

This method has then been used to determine the atomic concentration ratios [O]/[O_2] in the 4 mm diameter tube from the measurements of the intensities of the 844 and 777 nm lines and the values of C_{5P}^{2p1} and C_{3P}^{2p1} given in table 4. Results are represented in figure 10(*b*).

5. Recombination of oxygen atoms at the wall

In figure 10(*c*), we can observe a saturation of the [O]/[O_2] concentration ratio with increasing discharge currents for values above 50 and 20 mA for 7 and 4 mm diameter tubes respectively. We surmise that this saturation is due to the increase in the losses of oxygen atoms by recombination at the wall with increasing wall temperature. We have thus measured the temperature of the external wall of the tubes of different diameters and related the wall temperature to the recombination coefficient.

Table 4. Values of C_{5P}^{2p1} and C_{3P}^{2p1} calculated for the tubes of three diameters.

	Diameter (mm)			
	4	7	16	Mean value
C_{5P}^{2p1}	3.35×10^{-3}	3.44×10^{-3}	1.87×10^{-3}	2.78×10^{-3} ±55%
C_{3P}^{2p1}	2.78×10^{-3}	2.83×10^{-3}	2.10×10^{-3}	2.60×10^{-3} ±20%

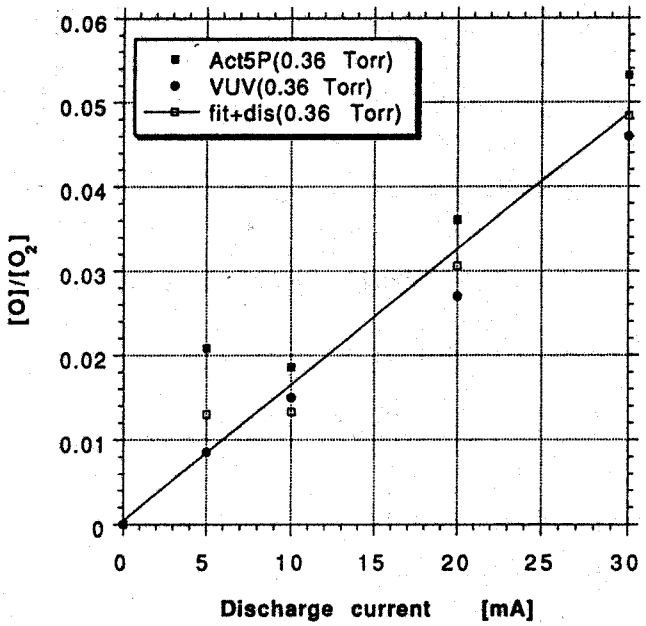

Figure 8. A comparison of $[O]/[O_2]$ measured by VUV absorption at 0.36 and 0.56 Torr and by actinometry taking into account the contribution of dissociative excitation of $O(^5P)$.

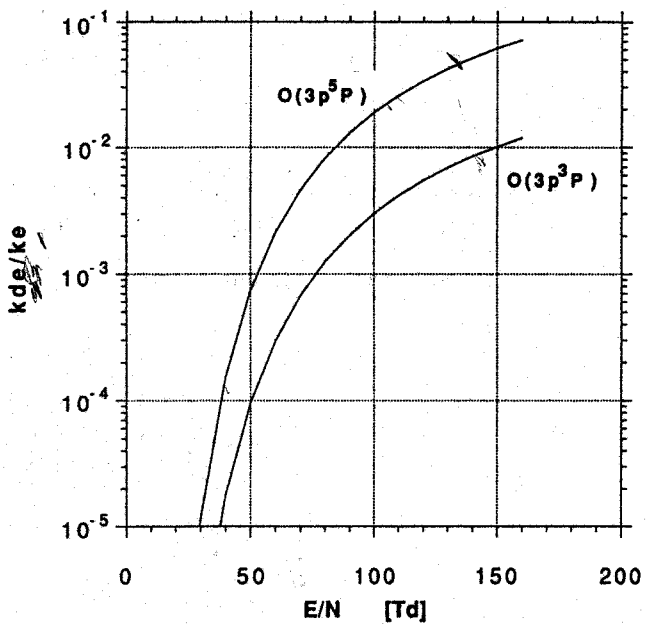

Figure 9. The ratio k_{de}/k_e of dissociative to direct excitation calculated for $O(3p\,^3P)$ and $O(3p\,^5P)$ states versus E/N.

In the discharge, the production of oxygen atoms in the ground state $O(2p^4\,^3P)$ is principally due to the dissociation of the molecule $O_2(X^3\Sigma_g^-)$ by electronic impact, according to the reactions

$$e + O_2(X^3\Sigma_g^-) \xrightarrow{k_{Diss}^{3P}} O(^3P) + O(^3P) + e \qquad (34)$$

$$e + O_2(X^3\Sigma_g^-) \xrightarrow{k_{Diss}^{1D}} O(^3P) + O(^1D) + e. \qquad (35)$$

Calculations of the k_{Diss}^{3P} and k_{Diss}^{1D} rate coefficients are performed using EEDFs and cross sections from Phelps [28] as indicated in relation (5). The total creation rate coefficient can be written

$$k_{Diss} = 2k_{Diss}^{3P} + k_{Diss}^{1D}. \qquad (36)$$

The loss of oxygen atoms in the ground state $O(2p^4\,^3P)$ is mainly due to atomic recombination at the wall [23]:

$$O(2p^4\,^3P) + \text{wall} \xrightarrow{k_{wall}} \tfrac{1}{2}O_2 \qquad k_{wall} = \frac{v_{Th}\gamma}{2R} \qquad (37)$$

where R is the discharge tube radius, γ the recombination probability and v_{Th} the thermal velocity of the oxygen atoms.

The radial profile of the gas temperature has been measured previously by CARS (coherent anti-Stokes Raman spectroscopy). It has been shown that the gas temperature near the wall is approximately the same as the wall temperature measured by a thermocouple [40]. We have then calculated v_{Th} assuming that the atom temperature is equal to the gas temperature at the wall. The balance between atomic oxygen production and loss is

$$[O(2p^4\,^3P)] = \frac{k_{Diss}}{k_{wall}} n_e [O_2]. \qquad (38)$$

If we express the mean value of electronic density n_e versus discharge current:

$$n_e = \frac{I_d}{\pi R^2 e v_D} \qquad (39)$$

where v_D is the electron drift velocity calculated as an electron transport parameter in the kinetic model of [20], then we can write the recombination probability as

$$\gamma = \frac{2I_d k_{Diss}}{\pi R e v_{Th} v_D} \frac{[O_2]}{[O]}. \qquad (40)$$

From the results of $[O]/[O_2]$ concentration ratios previously obtained by actinometry in the 4, 7 and 16 mm diameter tubes, we have calculated the values

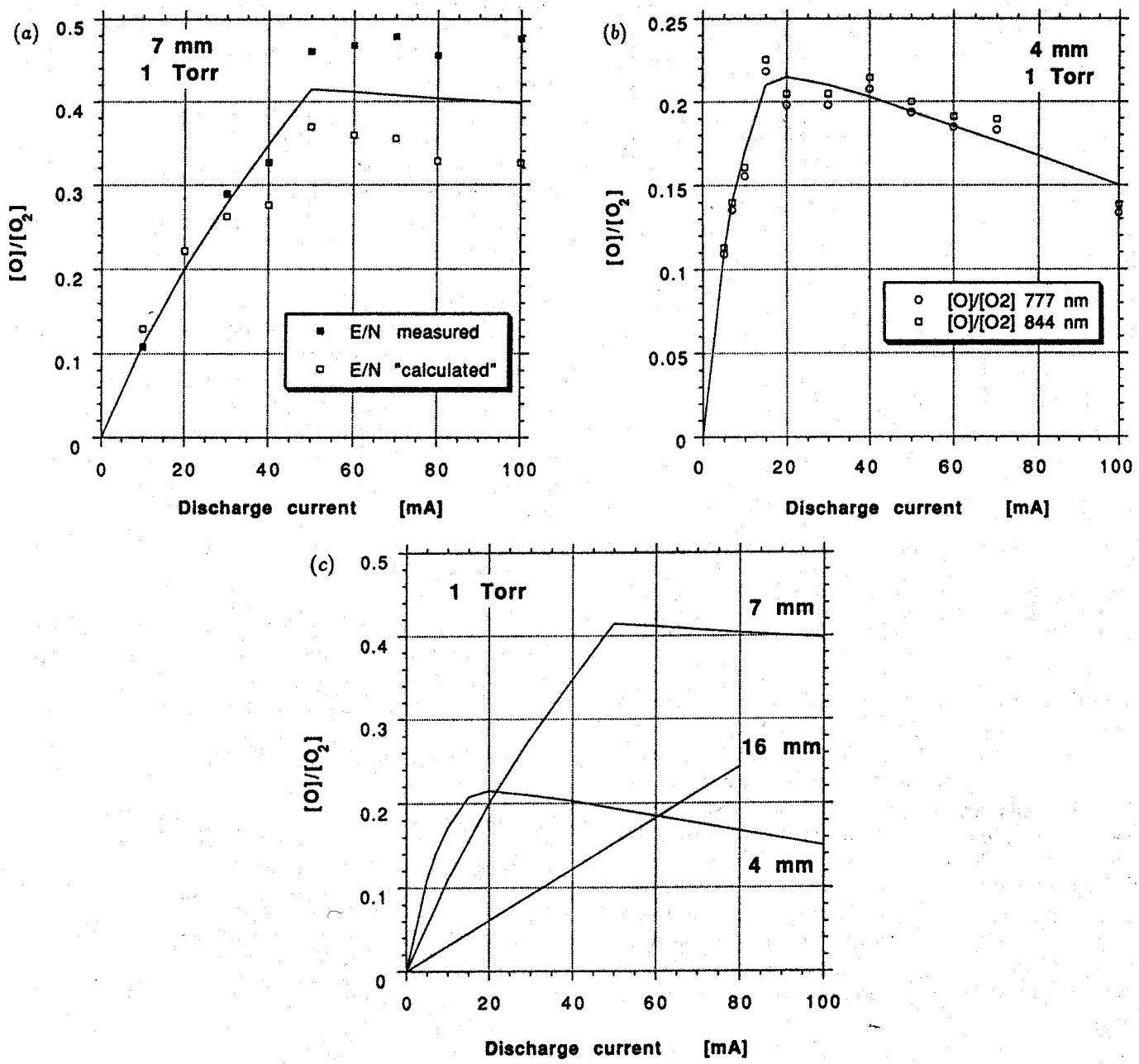

Figure 10. The $[O]/[O_2]$ dissociation ratio in 7, 4 and 16 mm diameter tubes versus discharge current for a pressure of 1 Torr. (*a*) For a 7 mm diameter tube: (■), values determined using the values of E/N measured by probes; and (○), values determined using E/N calculated from optical measurements. (*b*) For a 4 mm diameter tube, dissociation ratio determined using E/N calculated from optical measurements: (○), using the 777 nm line; and (□), using the 844 nm line. (*c*) A comparison of the results obtained in 4, 7 and 16 mm diameter tubes.

of γ under our experimental conditions of current and pressure for the three tube diameters. The results are represented in figure 11 versus $300/T_{wall}$, where T_{wall} is the wall temperature measured under the same experimental conditions. The variation of γ versus T_{wall} for the tubes of the three diameters can be fitted by the relation

$$\gamma = 0.94 \exp\left(-\frac{1780}{T_{wall}}\right). \tag{41}$$

It should be noted that the recombination of the oxygen atoms at the wall leading into the discharge Pyrex tube is larger than the values of γ ranging between 0.2×10^{-4} and 5×10^{-4} measured downstream of the discharge [41, 42]. This effect was first pointed out by Sabadil, who determined a recombination coefficient of $\gamma = 4.6 \times 10^{-4}$ within the discharge and $\gamma = 2.2 \times 10^{-4}$ outside the discharge. The values of γ measured in this work are five times larger. Nevertheless it is interesting to mention that the value $\gamma = 2.4 \times 10^{-3}$ measured at 300 K is in good agreement with the value determined by Magne [43] from the measurement of the atom concentration's time-dependence during the afterglow in a similar discharge tube. An explanation of this effect is proposed by the authors.

6. Conclusions

The validity of actinometric technique as a diagnostic tool for determination of absolute concentrations of atoms

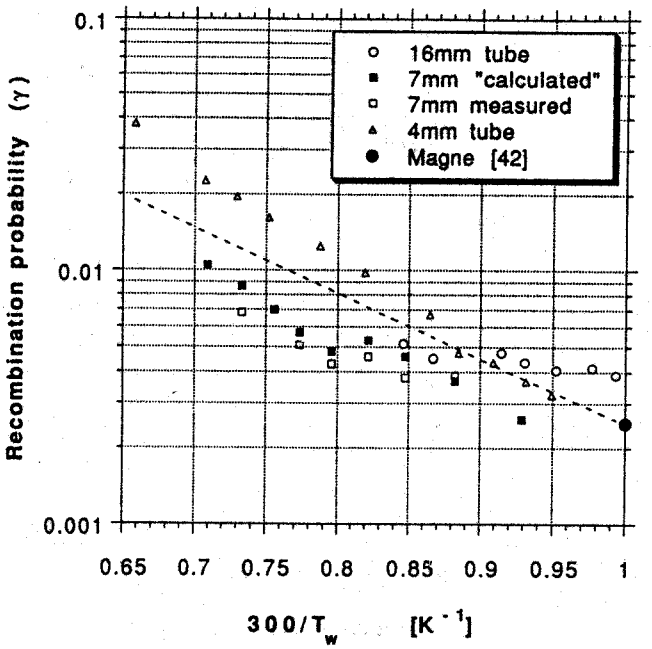

Figure 11. The variation of the recombination probability γ with the wall temperature T_{wall} for a 16 mm internal diameter tube (○), 7 mm internal diameter tube (□) and 4 mm internal diameter tube (△); (●), the value measured by Magne *et al* [42].

has been investigated. We have deduced the absolute concentration of oxygen atoms from the measurement of $O^*(^3P)/Ar^*(2p_1)$ and $O^*(^5P)/Ar^*(2p_1)$ emission intensity ratios. For this purpose we have calculated the rate coefficients for excitation of O* and Ar* versus reduced electric field using the calculated EEDF under our experimental conditions and several sets of cross sections. We have also studied the quenching of the emitted lines. By comparing the actinometric measurements to the results of VUV absorption spectrometry, we have demonstrated that the best choice of cross sections is the cross section of Puech [27] for $Ar^*(2p_1)$ and those of Laher [25] for $O^*(^3P)$ and $O^*(^5P)$.

Under these conditions, it has been shown that dissociative excitation can be neglected, except at low pressures and low currents. Under these experimental conditions in which $[O]/[O_2]$ is lower than 1% and the reduced electric field E/N is higher than 90 Td, dissociative excitation is a significant source of excited oxygen atoms, especially in the $O(^5P)$ state. However, it is possible to use actinometry for small concentrations of oxygen atoms if the contribution of dissociative excitation is taken into account in the calculations. When a large population of energetic electrons is present in the discharge, as in an ECR discharge, the contribution of dissociative excitation becomes too large to be corrected.

Furthermore, it has been shown that the reduced electric field can be deduced from the measurement of the intensity ratio. This allows a direct determination of the absolute concentration of oxygen atoms in discharge tubes of small diameter, where VUV absorption measurements are difficult to perform. It is to be noted that the transition $O(^3P–^3S)$ at 844 nm is a better choice for actinometric measurements because it can be used for a wide range of reduced electric fields (40–110 Td) and because the calibration factor $C_{3P}^{2p1} = 2.6 \times 10^{-3}$ ±20% remains constant when the pressures, the discharge currents and the tube diameters are varied.

In addition, we have shown that the concentration of oxygen atoms first exibits a linear variation with increasing discharge currents and then tends towards a saturation value. This saturation has been explained by the increase in the recombination of oxygen atoms at the wall, due to the increase in the Pyrex tube wall's temperature. A variation in the recombination probability $\gamma = 0.94\exp(-1780/T)$ has been determined for $300 < T < 500$ K. Work is in progress to determine the surface kinetics of oxygen atoms at the discharge tube wall.

This study allows one to conclude that the largest dissociation ratio is obtained in a 7 mm diameter discharge tube. Such a discharge tube has been used to build a source of oxygen atoms inserted into molecular beam epitaxy devices. The characteristics of this source will be published in the near future.

Acknowledgments

The authors would like to thank C M Ferreira, L Loureiro and V Guerra for providing the code for calculation of the EEDF, V Puech, J Bretagne and W Trennepohl for providing the cross sections for the excitation of argon and all of the above for helpful discussions. J Amorim and J Nahorny are supported by the CNPq, Brazil.

References

[1] Brink G O, Fluegge R A and Hull R J 1968 *Rev. Sci. Instrum.* **39** 1171
[2] Samson J A R and Pareek P N 1985 *Phys. Rev.* A **31** 1470
[3] Cuthbertson J W, Langer W D and Motley R W 1990 *Mater. Manufacturing Processes* **5** 387
[4] Collart E J H, Baggerman J A G and Visser R J 1991 *J. Appl. Phys.* **70** 5278
[5] Touzeau M, Schuhl A, Cabanel R, Luzeau P, Barski A, Pagnon D, Hirtz J P and Creuzet G 1989 *MRS Fall Meeting, Boston*
[6] Kwo J, Hong M, Trevor D J, Fleming R M, White A E, Farrow R C, Kortan A R and Short K T 1988 *In-situ* epitaxial growth of $Y_1Ba_2Cu_3O_{7-x}$ films by molecular beam epitaxy with an activated oxygen source *Appl. Phys. Lett.* **53** 2683
[7] Le Noxaïc A 1992 Hétéroépitaxie YSZ/Si élaboration par pulvérization ionique assistée par flux d'oxygène et caractérization" *Thèse doctorat* Université Paris-Sud Orsay
[8] Pagnon D, Amorim J, Nahorny J, Touzeau M and Vialle M 1991 Concentration of atoms in O_2 glow discharges by actinometry. Comparison with absolute measurements by VUV resonant absorption *Proc. ICPIG XX, Pisa* pp 1445–6
[9] Amorim J, Nahorny J, Pagnon D, Touzeau M and Vialle M 1991 Monitoring an oxygen atom source by actinometry *Proc. ISPC, Bochum*
[10] Pagnon D, Amorim J, Baravian G, Touzeau M and Vialle M 1994 Sources plasma d'atomes d'hydrogène et d'oxygène *Compte rendu du 4ème Congrès de la Section Plasma de la Société Française de Physique, Toulouse*
[11] Coburn J W and Chen M 1980 Optical emission spectroscopy of reactive plasmas: a method for

correlating emission intensities to reactive particle density *J. Appl. Phys.* **51** 3134
[12] De Benedictis S, Gicquel A and Cramarossa F 1987 N_2–H_2 radiofrequency plasma: role of H_2 on the vibrational kinetics of N_2 *Proc. 8th ISPC, Tokyo*
[13] Walkup R E, Saenger K L and Selwyn G S 1986 Studies of atomic oxygen in O_2 + CF_4 RF discharges by two-photon laser-induced fluorescence and optical emission spectroscopy *J. Chem. Phys.* **84** 2668
[14] Booth J P, Joubert O, Pelletier J and Sadeghi N 1991 Oxygen atoms actinometry re-investigated: comparison with absolute measurements by resonance absorption at 130.2 nm *J. Appl. Phys.* **60** 618
[15] Breithbarth F W, Ducke E and Tiller H J 1990 *Plasma Chem. Plasma Process.* **10** 377
[16] Granier Á, Chereau D, Henda K, Safari R and Leprince P 1994 Validity of actinometry to monitor oxygen atom concentration in microwave discharges created by surface wave in O_2–N_2 mixtures *J. Appl. Phys.* **75** 104
[17] Bouchoule A and Ranson P 1991 *J. Vac. Sci. Technol.* A **9** 317
[18] Hancock G, Sucksmith J P and Toogood M J 1990 *J. Phys. Chem.* **94** 3269
[19] Booth J P and Sadeghi N 1991 Oxygen and fluorine atom kinetics in electron cyclotron resonance plasmas by time-resolved actinometry *J. Appl. Phys.* **70** 611
[20] Gousset G, Ferreira C M, Pinheiro M, Sà P A, Touzeau M, Vialle M and Loureiro J 1991 Electron and heavy-particle kinetics in the low pressure oxygen positive column *J. Phys. D: Appl. Phys.* **24** 290–300
[21] Piétré S 1990 Utilization de l'actinométrie comme nouvelle méthode d'études des mécanismes de recombinaison catalytiques de l'oxygène atomique dans les plasmas d'air hors équilibre. Application au SiC–SiC, matériau candidat au système de protection thermique de l'avion spatial Hermès' *Thèse doctorat* Université Pierre et Marie Curie, Paris VI
[22] Gousset G, Panafieu P, Touzeau M and Vialle M 1987 Experimental study of a DC oxygen glow discharge by VUV absorption spectroscopy *Plasma Chem. Plasma Process.* **7** 409
[23] Gousset G, Touzeau M, Vialle M and Ferreira C M 1989 Kinetic model of a DC oxygen glow discharge *Plasma Chem. Plasma Process.* **9** 189
[24] Lefebvre M, Péalat M, Gousset G, Touzeau M and Vialle M 1990 Vibration kinetics of oxygen by CARS *ESCAMPIG X, Orléans* p 246
[25] Laher R R and Gilmore F R 1990 Updated excitation and ionization cross sections for electron impact on atomic oxygen *J. Phys. Chem. Ref. Data* **19** 277
[26] Schulman M B, Sharpton F A, Shung S, Lin C C and Anderson L W 1985 Emission from oxygen atoms produced by electron-impact dissociative excitation of oxygen molecules *Phys. Rev.* A **32** 2100
[27] Puech V and Torchin L 1986 *J. Phys. D: Appl. Phys.* **19** 2309–23
[28] Phelps A V 1985 Technical report 28, JILA Information Center, University of Colorado, Boulder
[29] Hall R I and Trajmar S 1975 *J. Phys. B: At. Mol. Phys.* **8** L293
[30] Henry R J, Burke P G and Sinfailan A L 1969 Scattering of electrons by C, N, O, N^+, O^+ and O *Phys. Rev.* A **178** 218–25
[31] Stone R J W and Zipf E C 1971 *Phys. Rev.* A **4** 610
[32] Fite W L and Brackmann R T 1959 *Phys. Rev.* **113** 815
[33] Drawin H W 1967 Report EUR-CEA-FC, Technical report 383, Commissariat à l'Energie Atomique, Fontenay-aux-Roses
[34] Julienne P S and Davis J 1976 Cascade and radiation trapping effects on atmospheric atomic oxygen emission excited by electron impact *J. Geophys. Res.* **81** 1397
[35] Ballou J K, Lin C C and Fajen F E 1973 Electron-impact excitation of the argon atom *Phys. Rev.* A **8** 1797
[36] Dagdigian P J, Forch B E and Miziolek A W 1988 Collisional transfer between and quenching of the $3p\,^3P$ and ^5P states of the oxygen atoms *Chem. Phys. Lett.* **148** 299
[37] Bamford D J, Jusinski L E and Bischel W K 1986 Absolute two-photon absorption and three-photon ionization cross sections for atomic oxygen *Phys. Rev.* A **34** 185
[38] Bittner J, Kohse-Höinghaus K, Meier U and Just T 1988 Quenching of two-photon-excited H(3s, 3d) and $O(3p\,^3P_{2,1,0})$ atoms by rare gases and small molecules *Chem. Phys. Lett.* **143** 571
[39] Belikov A E, Kusnetsov O V and Sharafutdinov R G 1995 The rate of collisional quenching of N_2O^+ ($B^2\Sigma$), N_2^+ ($B^2\Sigma$), O_2^+ (b $^4\Sigma$), O^+ (3d), O(3p), Ar^+ (4p′), Ar (4p, 4p′) at the temperature $\leq$ 200 K *J. Chem. Phys.* **102** 2792–801
[40] Touzeau M, Vialle M, Zellagui A, Gousset G, Lefebvre M, and Pealat M 1991 Spectroscopic temperature measurements in oxygen discharge *J. Phys. D: Appl. Phys.* **24** 41–7
[41] Wickramanayaka S, Hosokawa N and Hatanaka Y 1991 Variation of the recombination coefficient of atomic oxygen on pyrex glass with applied RF power *Japan. J. Appl. Phys.* **30** 2897–900
[42] Sabadil H and Pfau S 1985 Measurements of the degree of dissociation in oxygen DC discharges: comparison of the ozone method with the Wrede–Harteck method *Plasma Chem. Plasma Process.* **5** 67–79
[43] Magne L, Coitout H, Cernogora G and Gousset G 1993 Atomic oxygen recombination at the wall in a time afterglow *J. Physique* III **3** 1871–89